TNO report
PML 1996-A79

Computer simulations of the electrothermal behaviour of armatures during electromagnetic launch
Part 3: Miscellaneous 2-D simulation results

TNO Prins Maurits Laboratory

Lange Kleiweg 137
P.O. Box 45
2280 AA Rijswijk
The Netherlands

Phone +31 15 284 28 42
Fax +31 15 284 39 59

Date
November 1996

Author(s)
Dr. A.J. Schoolderman

Classification

Classified by	:	LKol. E.J.H. Elstak
Classification date	:	November 14, 1996 (this classificationwill not change)
Title	:	Ongerubriceerd
Managementuittreksel	:	Ongerubriceerd
Abstract	:	Ongerubriceerd
Report text	:	Ongerubriceerd

Copy no.	:	12
No. of copies	:	30
No. of pages	:	42 (excl. RDP & distribution list)
No. of annexes	:	-

All information which is classified according to Dutch regulations shall be treated by the recipient in the same way as classified information of corresponding value in his own country. No part of this information will be disclosed to any party.

The classification designation Ongerubriceerd is equivalent to Unclassified.

TNO Prins Maurits Laboratory is part of
TNO Defence Research which further consists of:

TNO Physics and Electronics Laboratory
TNO Human Factors Research Institute

Netherlands Organization for
Applied Scientific Research (TNO)

DISCLAIMER NOTICE

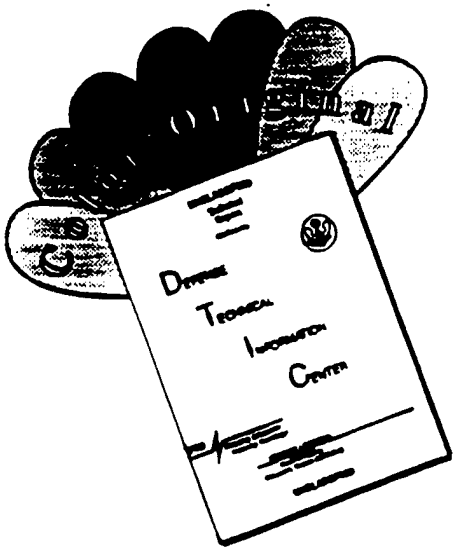

THIS DOCUMENT IS BEST QUALITY AVAILABLE. THE COPY FURNISHED TO DTIC CONTAINED A SIGNIFICANT NUMBER OF COLOR PAGES WHICH DO NOT REPRODUCE LEGIBLY ON BLACK AND WHITE MICROFICHE.

Managementuittreksel

Titel	:	Computer simulations of the electrothermal behaviour of armatures during electromagnetic launch Part 3: Miscellaneous 2-D simulation results
Auteur(s)	:	Dr. A.J. Schoolderman
Datum	:	november 1996
Opdrachtnr.	:	A87KL046
Rapportnr.	:	PML 1996-A79

Dit rapport is het vervolg op de TNO-rapporten PML 1991-80 'Computer simulations of the electrothermal behaviour of armatures during electromagnetic launch. Part 1: Solid, one-component armatures' en PML 1993-A77 'Part 2: Multi-fibre solid brush armatures'. Sinds 1987 worden bij het Laboratorium voor Pulsfysica van het TNO Prins Maurits Laboratorium fiber armaturen onderzocht in elektromagnetische versnelexperimenten teneinde tijdens schieten met een elektrisch energie kanon een vonkerosie-vrije lancering van het projectiel bij een zo hoog mogelijke snelheid te bereiken. Er wordt gestreefd naar mondingssnelheden in de orde van 2,5 tot meer dan 3 km/s, zodat een elektromagnetisch kanon ingezet kan worden voor antipantser- en luchtverdedigingsdoeleinden. Met behulp van het eindige-elementen computerprogramma ET-code, waarmee het elektrothermische gedrag van monoblok en fiber armaturen tijdens het versnelproces gesimuleerd kan worden, zijn verschillende armatuurvormen en armaturen van verschillende materialen bestudeerd. Het computerprogramma maakt gebruik van een tweedimensionaal model van de versneller en de armatuur. Door de voor- en nadelen van verschillende armatuurconcepten met simulaties te onderzoeken, kunnen experimenten gerichter en dus efficiënter worden uitgevoerd.
In dit rapport wordt een aantal recente resultaten van simulaties van het elektrothermische gedrag van fiber armaturen tijdens een elektromagnetisch versnelproces gepresenteerd alsmede drie uitbreidingen van het programma ET-code. Deze uitbreidingen betreffen de mondingsspanningsberekening, een simpel model voor de transitie van de armatuur en een model voor de opwarming ten gevolge van wrijving. Er zijn drie methoden onderzocht die mogelijk resulteren in een betere stroomverdeling in de armatuur tijdens het versnelproces, namelijk het gebruik van rails met een resistieve laag, fiber armaturen met fiber uiteinden van een ander materiaal dan het bulkmateriaal en het vergroten van de lengte van de armatuur. Het gebruik van een resistive laag leidt bij monoblok armaturen inderdaad tot een betere verdeling van de stroom. De mate waarin dit gebeurt is afhankelijk van de laagdikte en de resistiviteit van het materiaal. Voor fiber armaturen is geen eenduidige conclusie mogelijk.
Bij het gebruik van fiber armaturen met fiber uiteinden van een materiaal met een hoger elektrisch geleidingsvermogen dan de rest van de armatuur wordt de stroomverdeling bepaald door de eigenschappen van het bulkmateriaal. Wanneer fiber

armaturen met fiber uiteinden van een materiaal met een elektrisch geleidingsvermogen lager dan de rest van de armatuur worden gebruikt, begint het armatuurmateriaal al in een vroeg stadium van het versnelproces te smelten.
Met behulp van een nieuw ontwerp voor fiber armaturen, het zogenaamde gesegmenteerde fiber armatuur, is de invloed op de stroomverdeling in U-vormige koperen en molybdenen fiber armaturen tijdens het versnelproces onderzocht. Er is een optimale armatuurlengte voor koperen gesegmenteerde fiber armaturen gevonden: als de armatuur waarvan de lengte gelijk is aan deze optimale lengte nog verder verlengd wordt, heeft dat geen invloed op de stroomverdeling in de armatuur. Koperen gesegmenteerde fiber armaturen met een lengte gelijk aan deze optimale armatuurlengte worden in het Laboratorium voor Pulsfysica gebruikt in elektromagnetische versnelexperimenten. Gesegmenteerde fiber armaturen van molybdeen hebben waarschijnlijk een grotere optimale armatuurlengte dan in verband met de lanceerpakketmassa praktisch realiseerbaar is.
Uit de berekeningen van de spanning over de monding van de railversneller met behulp van de in dit rapport beschreven methode volgt dat de inductieve bijdragen aan deze spanning alleen van belang zijn als de stroom zeer snel in de tijd verandert. Hoewel in de simulaties gebruik wordt gemaakt van een twee-dimensionaal model van de versneller en de armatuur, komen de berekende mondingsspanningsprofielen goed overeen met de gemeten mondingsspanningen in armatuurtestbedexperimenten en versnelexperimenten met fiber armaturen. Met behulp van een simpel model voor de armatuurtransitie, gebaseerd op het 'melt-wave' concept, is aangetoond dat de snelle stijging van de mondingsspanning die waargenomen is tijdens een zeker versnelexperiment, uitgevoerd in het Laboratorium voor Pulsfysica, waarschijnlijk niet het gevolg is van armatuurtransitie veroorzaakt door alleen maar Ohmse opwarming.
Uit onderzoek van de overblijfselen van fiber armaturen die na versnelexperimenten zijn opgevangen is geconcludeerd dat de uiteinden van de fibers tijdens het versnelproces smelten. Deze conclusie wordt onderschreven door de resultaten van computersimulaties met ET-code indien, naast Ohmse opwarming en het smelten van de isolatie van de fibers, ook de opwarming ten gevolge van wrijving meegenomen wordt. In de modellen voor de armatuurtransitie en voor hybride armaturen die in het vervolg van het elektromagnetisch versnelonderzoek ontwikkeld zullen worden, zal ook de opwarming en het smelten van armatuurmateriaal door de wrijvingswarmte moeten worden beschouwd.

Contents

1 Introduction

This report is the sequel to the TNO-reports PML 1991-80, 'Computer simulations of the electrothermal behaviour of armatures during electromagnetic launch. Part 1: Solid, one-component armatures' [1] and PML 1993-A77, 'Computer simulations of the electrothermal behaviour of armatures during electromagnetic launch. Part 2: Multi-fibre solid brush armatures' [2].
In the former, the computer code ET-code, originally developed by G.C. Long [3], is described extensively. This code is based on the finite element method and has been developed especially to study the electrothermal behaviour of solid armatures during electromagnetic launch. To this end, a 2-dimensional representation of the accelerator and armature is used. A number of simulations of the behaviour of rectangular and U-shaped monobloc armatures made of copper, aluminum or molybdenum, executed with ET-code, are included in [1].
In the latter, the extention of the code with an option for the simulation of the electrothermal behaviour of multi-fibre solid brush armatures (abbreviated: fibre armatures) is introduced. It is particularly this type of armature that is studied experimentally at the Pulse Physics Laboratory of TNO Prins Maurits Laboratory (TNO-PML). In the model used for the fibre armatures, the armature is considered to be made of a material with an anisotropic resistivity and thermal conduction. In [2], simulation results of the electrothermal behaviour for fibre armatures with different shapes and materials are given. The influence of the degradation of the electrical insulation of the fibres during launch is also studied. The most salient results from this report were presented at the 4th European Symposium on Electromagnetic Launch Technology, Celle, Germany in 1993 [4] and the 7th Symposium on EML Technology, San Diego, USA in 1994 [5].
In the present report, the results of simulations with the 2-dimensional electrothermal computer code ET-code of acceleration processes with resistively layered rails, armatures of fibres tipped with various materials and segmented fibre armatures are presented. The influence of the use of rails with a layer of a resistive material and fibre armatures with fibre tips of a different material than the bulk of the armature on the current density in the armature is studied. The optimal armature length of copper and molybdenum fibre armatures is determined by means of a new fibre armature type, the segmented fibre armature. With this fibre armature type it is possible to lengthen the armature without affecting the shape of the fibres. The computer code is extended with a model for the calculation of the muzzle voltage during the acceleration of solid fibre armatures. With a crude model for the transition of a solid fibre armature to a hybrid armature - the melt-wave model - the origin of an experimentally observed transition is studied. Finally, the computer code is extended with a model for the heating of the armature due to friction. With the results of simulations with this model the experimentally observed melting of parts of the fibre in a fibre armature at the rail-armature interface during launch can be explained.

2 Launch performance predictions of an accelerator with resistively layered rails

It has been claimed by several authors that high transition velocities of armatures in rail accelerators can be achieved when monobloc armatures in combination with rails with a resistive layer are applied in electromagnetic launching [6], [7], [8]. The resistive layer forces the current to penetrate deeper into the armature, so that the current density at its trailing edge is lower. In contrast to this, it has been found in computer simulations that the performance of 'modified chevron' armatures, which consist of insulated leafs of, for example, copper or molybdenum with a thickness of approximately 1.0 mm, with resistive rails (molybdenum layer on copper rails) is worse than with homogeneous copper rails, due to increased heating on the rail side of the rail-armature interface [3], [9]. However, no monobloc armatures or fibre armatures have been considered there.
In order to be able to compare results of our simulations executed with the computer code 'ET-code' (see [1] and [2] for an extenstive description of this code) with the predictions stated in [6], simulations of the magnetic field distribution in rectangular copper monobloc armatures and fibre armatures (with packing fraction r = 1) accelerated along copper rails with a resistive layer, were executed. The armature velocity and the breech current were taken as constant and the total thickness of the rail was 17.6 mm. The skin depth, which describes the penetration of the magnetic field into the armature in the direction of the motion (see [1]), was calculated after 3 ms, i.e. after a stationary field distribution is obtained. Several resistivities ρ_{rl} of the resistive layer and thicknesses w of the resistive layer were considered. In these simulations, the temperature rise due to Joule heating was not taken into account. The calculated values of the skin depth for an armature velocity of 500 m/s are given in Figure 2.1 (for monobloc armatures) and Figure 2.2 (for fibre armatures). For a rectangular copper monobloc armature, the optimal thickness-resistivity combination for the layer is found to be w = 1 mm and $\rho_{rl} = 100\rho_{Cu}$ for an armature velocity v = 500 m/s. When a smaller resistivity of the layers is chosen, the optimal layer thickness decreases, but the effect of the presence of a resistive layer on the current distribution in the armature reduces. For a lower armature velocity, thicker rail layers should be applied (see Figure 2.3). These statements agree with the predictions in [6]. For rectangular copper fibre armatures, the rail layer thickness-resistivity combinations considered have only a positive effect on the current density in the armature at low velocities (e.g. 100 m/s). This is illustrated in Figure 2.3 for a resistive layer with a resistivity of 50 times the resistivity of copper. Moreover, it is unexpectedly found that a rail layer with a lower resistivity than that of the armature, will also increase the skin depth (see Figures 2.1 and 2.2).

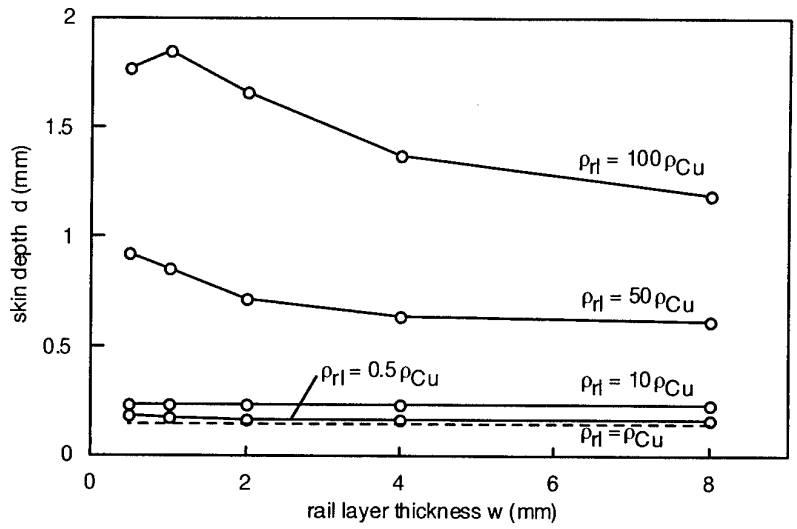

Figure 2.1: Skin depth in a rectangular copper monobloc armature at v = 500 m/s versus the resistive rail layer thickness w and resistivity ρ_{rl}. Joule heating is neglected.

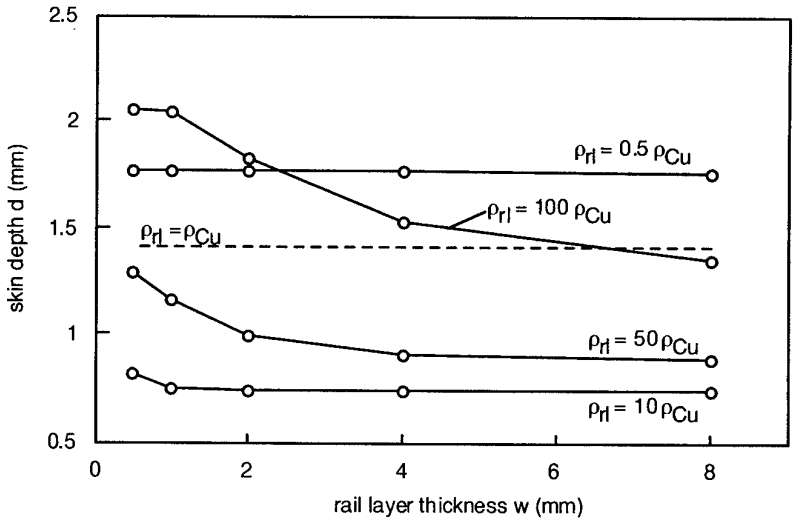

Figure 2.2: Skin depth in a rectangular copper fibre armature at v = 500 m/s. Joule heating is neglected.

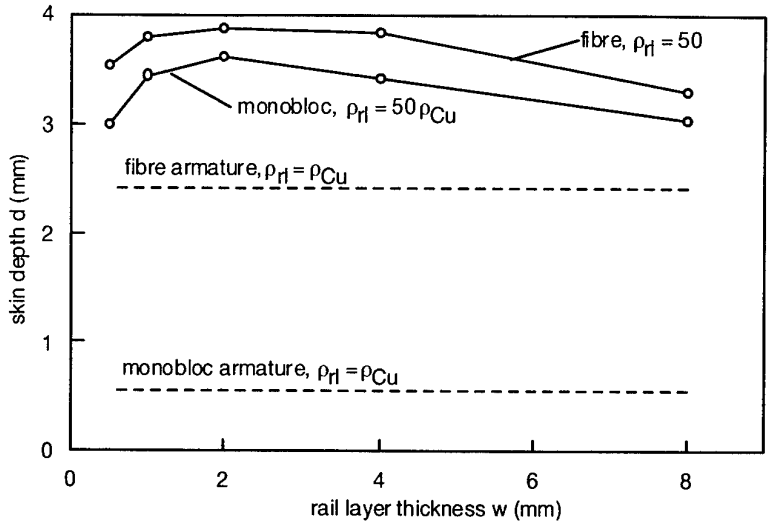

Figure 2.3: Skin depth in rectangular copper monobloc and fibre armatures at v = 100 m/s. Joule heating is neglected.

To study the effect of a resistive layer on the electrothermal behaviour of a U-shaped monobloc armature with a trailing edge angle of 45° during electromagnetic launch, a simulation was executed for a layer of 0.5 mm thickness and a resistivity 50 times that of copper (in the order of that of stainless steel). For this hypothetical layer material, values were chosen for the specific heat and the thermal conductivity equal to 0.5 and 0.1 times those of copper. The breech current and velocity profile used in this simulation is given in Figure 2.4.
In Figure 2.5, the maximum temperature and the skin depth in the armature during this simulated launch are compared with those during a launch where copper rails are applied. When resistive layers on the rails are used, it takes more time for the armature to arrive at its melting temperature. Then, the maximum temperature in the resistive layers during the launch is 893 °C.
Although the maximum temperature in the copper monobloc armature during a launch where resistive layers on the rails are used rises very quickly when the melting temperature of the armature is reached, the potential to achieve higher transition velocities for monobloc armatures under such conditions is clearly demonstrated. A general conclusion for the launch performance of fibre armatures in a rail accelerator with resistive rails is not possible because the current distribution in these armatures appears to be very sensitive to the armature velocity and the material properties of the resistive layer. Unfortunately, up to now no experimental results of launching with resistively layered rails are available.

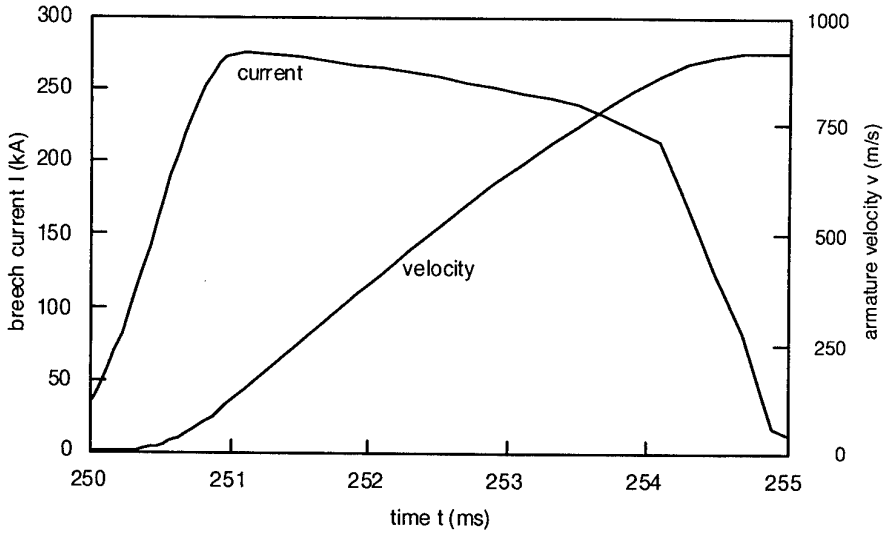

Figure 2.4: Current and armature velocity profile.

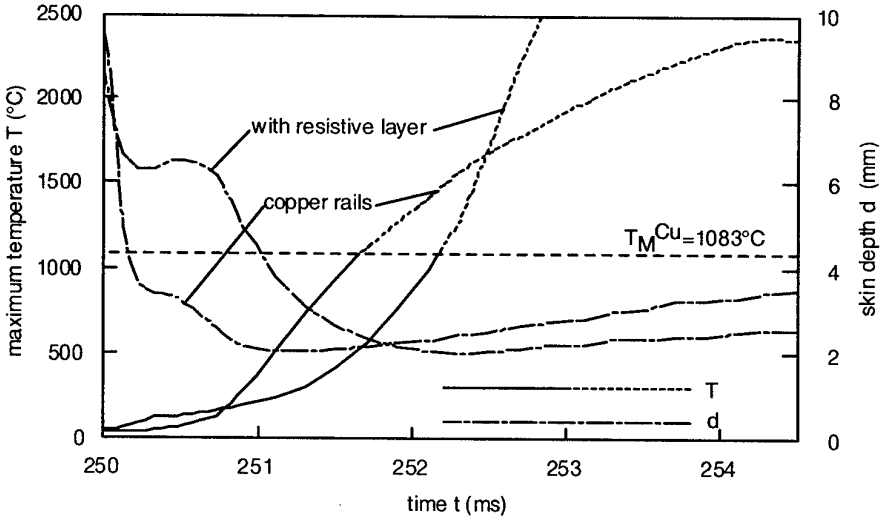

Figure 2.5: Maximum temperature T and skin depth d in a 45° copper monobloc armature during electromagnetic launch with homogeneous copper rails and with copper rails covered with a resistive layer.

3 Launch performance predictions of fibre armatures with fibre tips of a different material

In this chapter the electrothermal behaviour of multi-fibre solid brush armatures with fibre tips of a different material are studied by means of computer simulations. It is expected that a better current distribution in the armature during launch can be achieved by using fibres with tips made of a metal with a different resistivity than the bulk material. The results of these simulations are compared with the results of simulated launches with armatures consisting of fibres without tips of a different material.
In the simulations, electromagnetic launches of launch packages with a mass of 3.6 kg with a 90 mm square bore accelerator are considered. The U-shaped fibre armatures have a width of 64 mm and an interface length l of 22 mm or 31.1 mm. The trailing edge angle α is equal to 45°. The packing fraction r of the armatures is 70%. Figure 3.1 shows the geometry of these armatures. The direction of the electrically insulated fibres is parallel with the trailing side of the armature in all cases considered. The composition of the different fibre armatures which are studied in this chapter are summarized in Table 3.1.

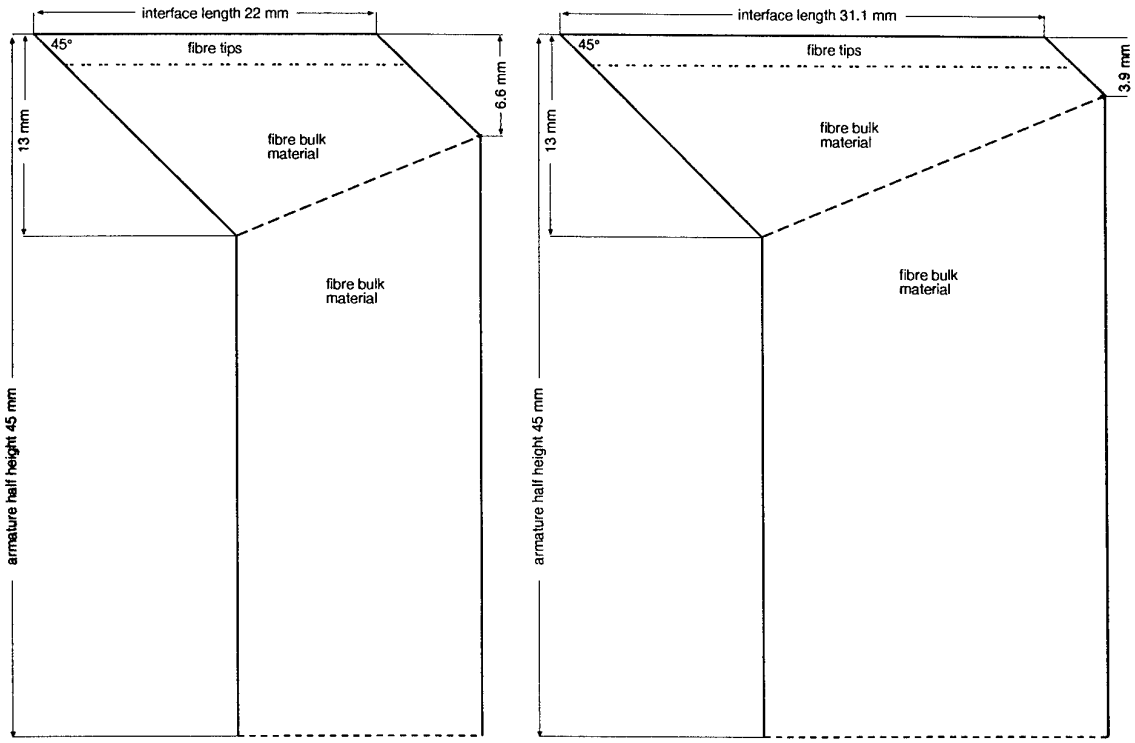

Figure 3.1: Geometry of the armatures with interface lengths l = 22 mm and l = 31.1 mm.

Table 3.1: Composition of the fibre armatures studied in this chapter.

bulk material	tip material	tip length	identification
interface length l = 22 mm			
Cu	Mo	0.5 mm	CuMo_0.5
Cu	Mo	1 mm	CuMo_1
Cu	Mo	2 mm	CuMo_2
Cu	Mo	13 mm *	CuMo_13
Cu	-	-	Cu_l22
Mo	-	-	Mo_l22
interface length l = 31.1 mm			
Mo	Cu	2 mm	MoCu_2
Mo	Al	2 mm	MoAl_2
Cu	-	-	Cu_l31.1
Mo	-	-	Mo_l31.1

* the total oblique part of the armature consists of molybdenum fibre tips

The current profile and the velocity profile used in the simulations are shown in Figure 3.1. The current increases to a constant value of 2.91 MA in 1 ms. The motion of the launch packages starts at t = 1 ms, i.e. when the current reaches its constant value.

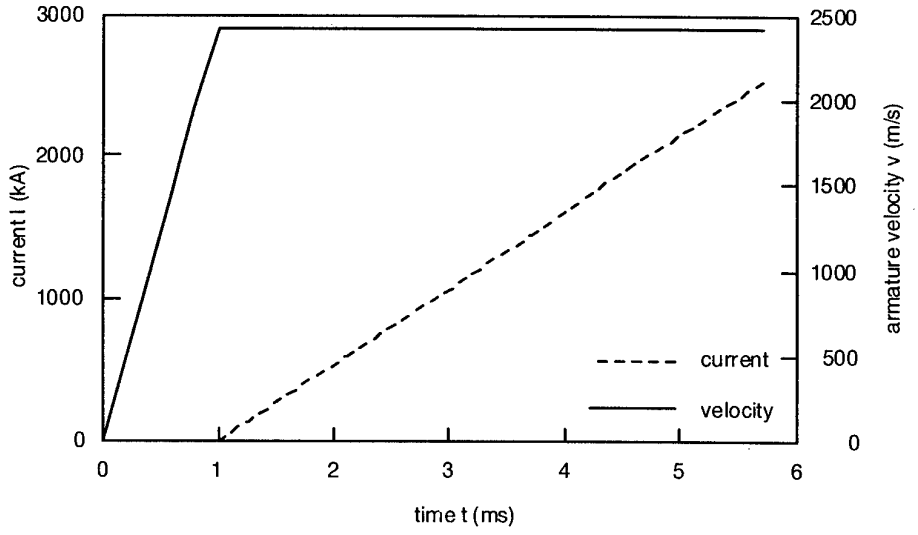

Figure 3.2: Current profile and armature velocity profile.

Figures 3.3 and 3.4 give the skin depth d during the simulated launch of the different armatures. The skin depth of the copper fibre armatures with molybdenum tips of 0.5 mm, 1 mm or 2 mm is greater than in the copper fibre armature without tipped fibres (Cu_l22). Hence, a more uniform current distribution is achieved in these tipped fibre armatures. However, in the copper bulk near the fibre tips, melting of copper already occurs before the launch package starts to move (i.e. before t = 1 ms). The highest temperature in these armatures occurs in the molybdenum tips. When longer molybdenum fibre tips are used, as in armature

CuMo_13, the skin depth increases. In this armature, the melting temperatures of the copper bulk and the molybdenum fibre tips are reached at nearly the same launch package velocity of 384 m/s. The skin depth in the fibre armatures with a copper bulk and molybdenum tips is greater than in a copper fibre armature with the same interface length.
From Figure 3.4 it is clear that the skin depth in fibre armatures with a molybdenum bulk and copper or aluminum fibre tips is determined by the properties of the bulk material. The melting of the molybdenum bulk of armature MoCu_2 starts when the launch package has a velocity of 930 m/s. Then the highest temperature in the copper fibre tips is 935 °C. In armature Mo_l31.1, the melting temperature of molybdenum is reached at a velocity of 957 m/s. It can be concluded that the copper fibre tips hardly change the electrothermal behaviour of the molybdenum fibre armatures. The melting temperature in the aluminum tips of armature MoAl_2 is reached when the launch package has a velocity of only 277 m/s. At that velocity the highest temperature in the molybdenum bulk of this armature is 1170 °C. Because of the melting of the aluminum fibre tips at an early stage of the acceleration process, these armatures are probably suitable to obtain a controlled transition of the solid armature to a hybrid armature, i.e. an armature which is partly solid and partly fluid (i.e. melted armature material), vapour or plasma. The melt behaviour of the studied armatures is summarized in Table 3.2.

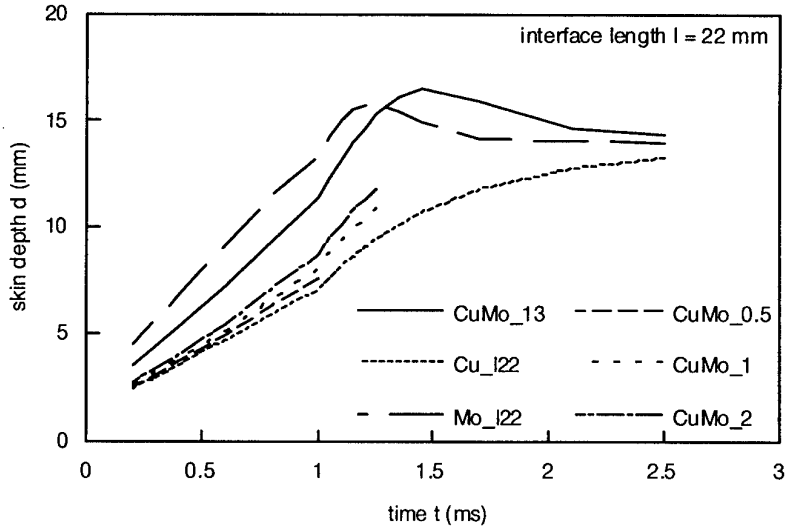

Figure 3.3: Skin depth d during launch for the fibre armatures with interface length l = 22 mm.

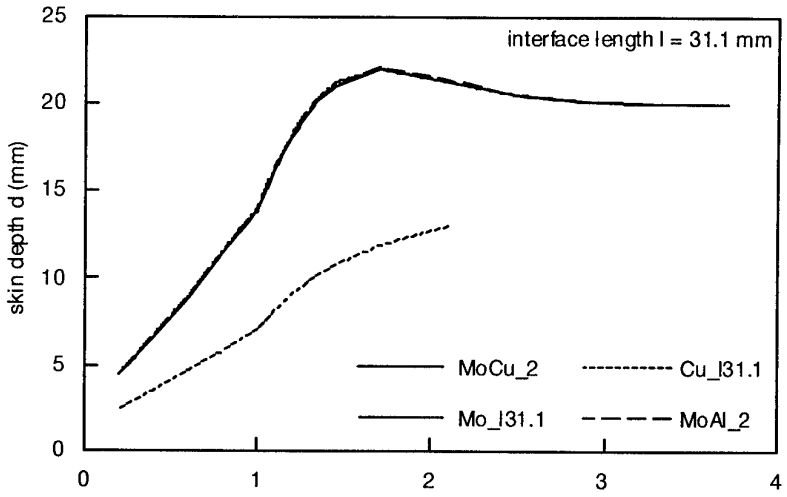

Figure 3.4: Skin depth d during launch for the fibre armatures with interface length l = 31.1 mm.

Table 3.2: Melt behaviour of the different fibre armatures.

identification	melting armature material	melting at velocity (m/s)
interface length l = 22 mm		
CuMo_0.5	Cu, near Mo tips	0
CuMo_1	Cu, near Mo tips	0
CuMo_2	Cu, near Mo tips	0
CuMo_13	Mo tips and Cu bulk at the same velocity	384
Cu_l22	Cu	352
Mo_l22	Mo	475
interface length l = 31.1 mm		
MoCu_2	Mo	930
MoAl_2	Al	277
Cu_l31.1	Cu	362
Mo_l31.1	Mo	957

4 The optimal armature length and segmented fibre armatures

To achieve high transition velocities in electromagnetic launch processes with solid armatures, a uniform current density in the armature during the launch is a prerequisite. However, the electromagnetic acceleration process is a strongly transient process and the penetration of the magnetic field into the armature is limited due to the transient nature of the process. Moreover, the velocity skin effect diminishes the magnetic field penetration during the acceleration process. In order to obtain a more uniform current distribution, different armature concepts, e.g. multi-fibre solid brush armatures, armature geometries, armature materials, etc., can be applied. In this chapter, the influence of the length of a fibre armature on the current distribution and the launch performance is studied and the existence of an 'optimal armature length' is investigated. The optimal armature length is the smallest length of an armature by which the most uniform current distribution is achieved during launch. In general, the optimal armature length will depend on the launch parameters (current profile, velocity profile, etc.) and the type of armature (geometry, material, etc.). Knowledge of the value of the optimal armature length is important for the design of launch packages, consisting of an armature, a sabot and the projectile, with a minimum parasitic mass.

In order to check the concept of an optimal armature length, simulations of launch processes with a new fibre armature geometry, the segmented fibre armature, are executed. The advantage of this geometry is that the armature can be composed of an arbitrary number of identical fibre armature segments and the interface length can be easily lengthened. Figure 4.1 shows one half of the armature geometry and the element mesh used in the simulations of a segmented fibre armature consisting of 5 segments. The interface length of one segment is 7.425 mm. The armature width is equal to 20 mm. The spaces between the segments (the red areas in Figure 4.1) are filled up with an electrically and thermally insulating material. In experimentally studied segmented fibre armatures, these spaces can be filled up with G10, for example.

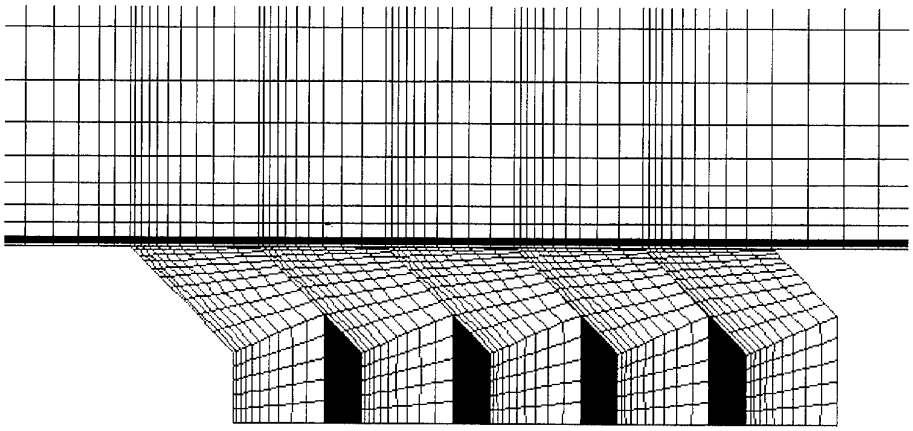

Figure 4.1: Geometry and element mesh used in the simulation of the launch process with a segmented fibre armature consisting of 5 segments.

Launch processes with a 20 mm square bore accelerator are simulated. The current profile and the velocity profile used in the simulations are shown in Figure 4.2. It is assumed that all launch packages accelerated with the considered segmented armatures have the same mass.

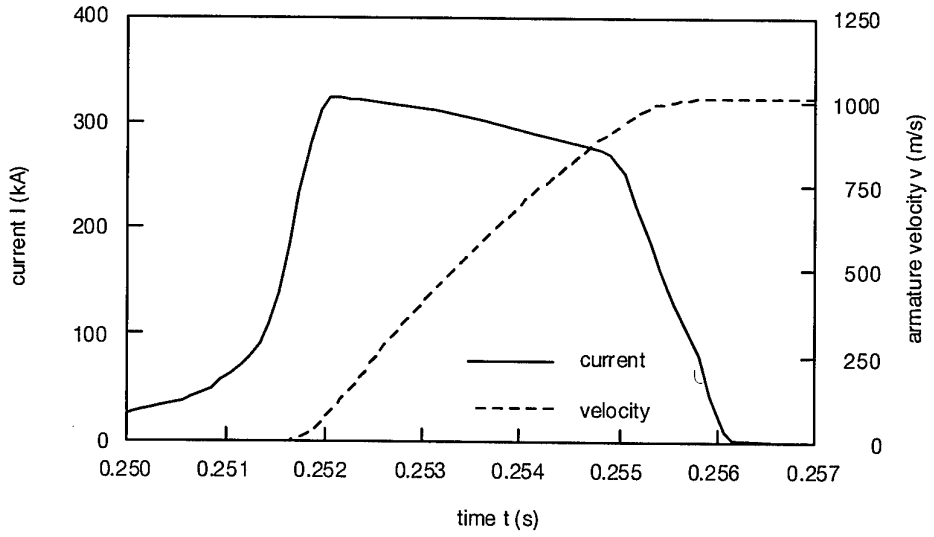

Figure 4.2: Current and velocity profile.

Figures 4.3 and 4.4 give the velocity, the skin depth and the highest temperature in the armatures during the simulated launches with copper segmented fibre armatures consisting of 1, 2, 3, or 4 segments. From these figures it can be concluded that the optimal armature length for copper segmented fibre armatures lies between 7.425 mm and 14.85 mm. When more segments are added to a copper segmented fibre armature with 2 segments, almost no current will flow through the added

segments and the transition velocity will not change (provided that the launch package mass of the armature is the same).

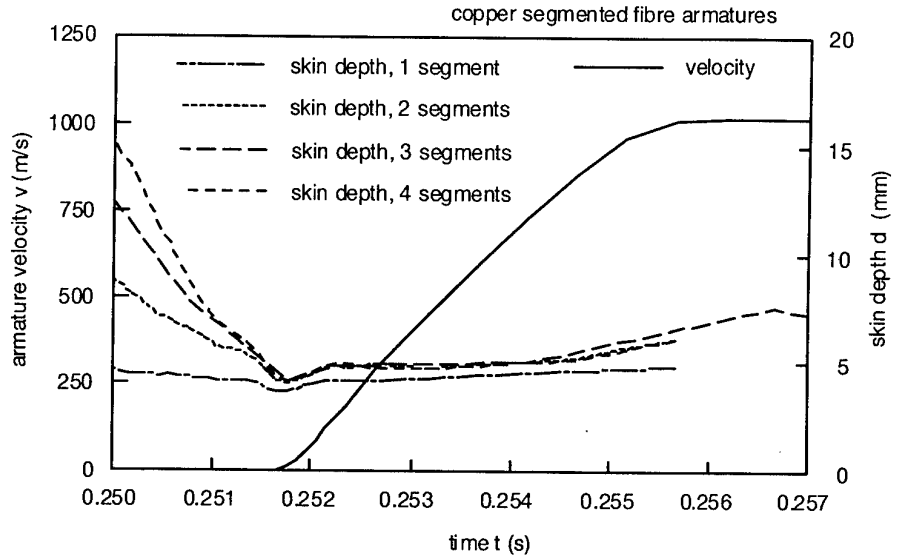

Figure 4.3: Velocity and skin depth during the simulated launch process of copper segmented fibre armatures consisting of 1, 2, 3 or 4 segments.

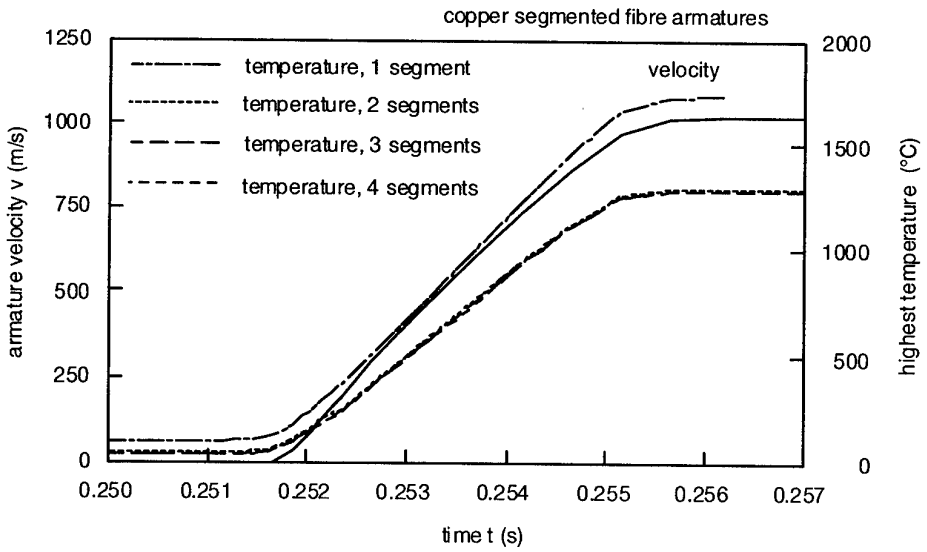

Figure 4.4: Velocity and highest temperature occurring in the copper segmented fibre armatures consisting of 1, 2, 3 or 4 segments. The temperature curves for the armatures of 3 and 4 segments coincide.

For the molybdenum segmented fibre armatures consisting of 1, 2, 3, 4 or 5 segments, the velocity, the skin depth and the highest temperature in the armatures are shown in Figures 4.5 and 4.6. The temperature in the molybdenum segmented fibre armatures with 1 or 2 segments increases very quickly due to the high current

density in these armatures and the relatively high resistivity of molybdenum (the resistivity of molybdenum is approximately 3.6 times the resistivity of copper). The temperature in the molybdenum segmented fibre armature with 3 segments does not reach the melting temperature of molybdenum during the simulated launch. Figures 4.7 and 4.8 show the current distributions at t = 0.25415 s in the copper and molybdenum segmented fibre armatures consisting of 3 segments. In each of the nine coloured belts 10% of the current flows; the last 10% flows in the uncoloured area. When 1 or 2 segments are added to the molybdenum segmented fibre armature with 3 segments, the skin depth increases and the highest temperature in the armature during the launch decreases with approximately 200 °C and 400 °C, respectively. A significant amount of current flows through the added segments. We conclude that the optimal armature length of molybdenum segmented fibre armatures is longer than 37.125 mm for the launch parameters considered here.

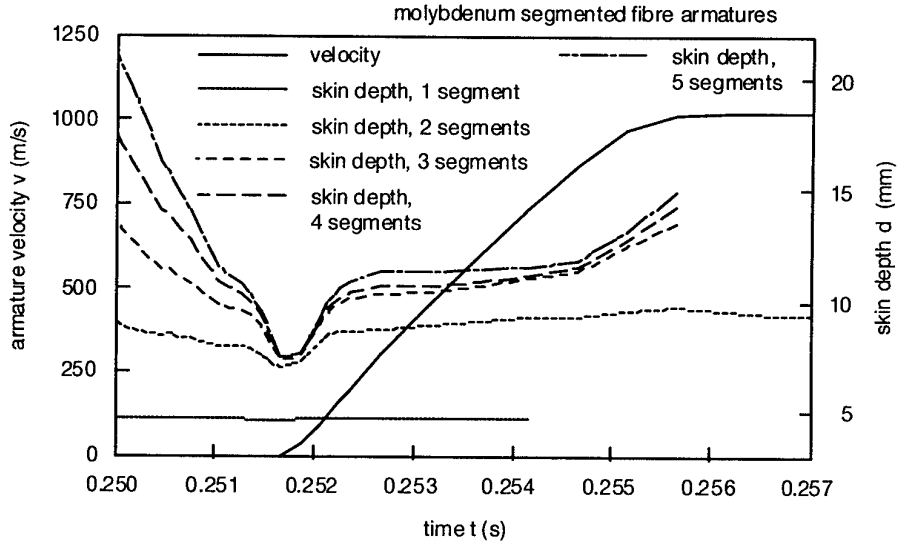

Figure 4.5: Velocity and skin depth during the simulated launch process of molybdenum segmented fibre armatures consisting of 1, 2, 3, 4 or 5 segments.

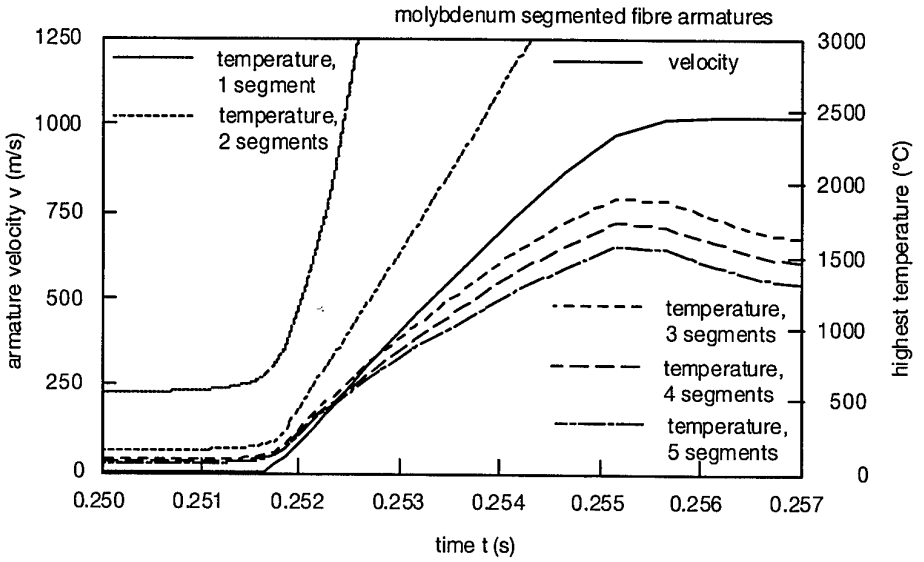

Figure 4.6: Velocity and highest temperature occurring in the molybdenum segmented fibre armatures consisting of 1, 2, 3, 4 or 5 segments.

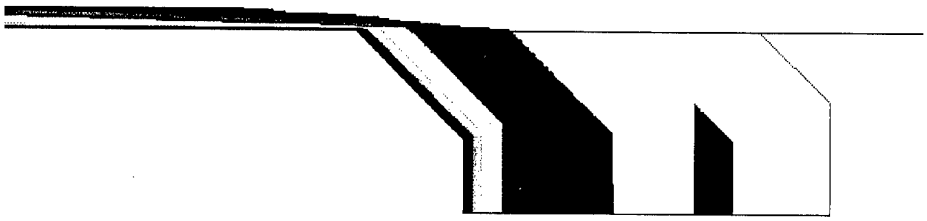

Figure 4.7: Current distribution in the segmented copper fibre armature consisting of 3 segments at t = 0.25415 s (v = 729.6 m/s).

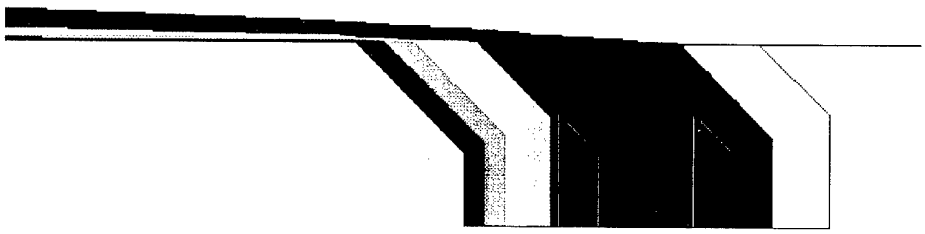

Figure 4.8: Current distribution in the segmented molybdenum fibre armature consisting of 3 segments at t = 0.25415 s (v = 729.6 m/s).

5 Muzzle voltage calculations

In electromagnetic launch experiments with solid armatures, the muzzle voltage measurement is an important diagnostic means: a rapid change of the muzzle voltage characterises the transition of a solid armature to a hybrid one. In the first three sections of this chapter, we will focus on the muzzle voltage during the process of acceleration of solid fibre armatures. In section 5.4, a very simple model for the armature transition is described. This model is incorporated in the 2-dimensional electrothermal finite element computer code ET-code to demonstrate the use of the muzzle voltage as a diagnostic means. Probably in the future, when the computer code is extended with a more realistic (and possibly validated) model for the transition process, the model developed for the calculation of the muzzle voltage can be used for the comparison of the performance of different transitioning solid armatures.

5.1 Method

A formula for the muzzle voltage $V_m(t)$ can be derived by integrating Faraday's equation over the closed surface O and applying Stokes's theorem

$$\int_C E \cdot dl = -\int_O \frac{dB}{dt} \cdot dO \tag{5.1}$$

The closed contour of the surface O is denoted by C. The left-hand side of this equation can be written as the voltage drop over the leading end of the rails, i.e. the muzzle voltage, and an integral over the electric field along path C' from A to B (see Figure 5.1)

$$V_m = \int_{C'} E \cdot dl + \int_O \frac{dB}{dt} \cdot dO \tag{5.2}$$

In Figure 5.1, two paths, C'_1 and C'_2, are shown. Both paths run along the inside of the rails; path C'_1 is chosen along the front edge of the armature and C'_2 along the rail-armature interface and the trailing edge of the armature.

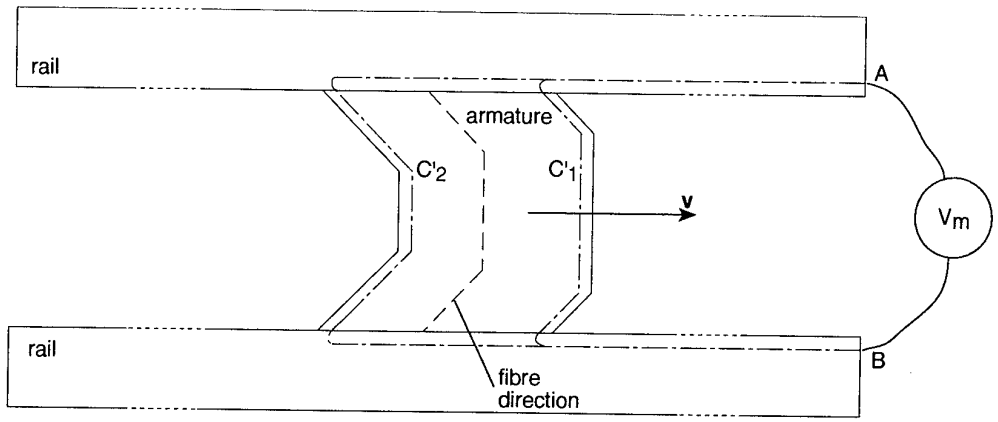

Figure 5.1 Layout of the 2-D representation of the rail accelerator and the multi-fibre solid brush armature.

With the finite element computer code ET-code, the electric field **E** and the magnetic induction **B** in fibre armatures can be calculated in the two-dimensional representation of the accelerator, i.e. in the plane at half-height of the rails, during the launch process [1], [2], [4], [5]. In the 2-D picture, the magnetic field in front of the armature (i.e. at the muzzle side) is set equal to zero. Hence, the second term on the right-hand side of eq. (5.2), i.e. the induction contributions to the muzzle voltage, will disappear for contour C_1. In order to estimate the value of this induction contribution, the magnetic field in this region due to the current distribution in the armature is calculated with the help of Biot-Savart's law. Since the value of the inductance in the 2-D representation of the rail accelerator, L_2, is different from the actual value of the inductance, L_3, it is not expected that this procedure will yield the exact value of this induction contribution.

5.2 Comparison with Hughes and Young's calculation

In 1982, a paper by Hughes and Young was published in which they presented the derivation of an integro-differential equation which governs the magnetic field distribution in rectangular multi-fibre solid brush armatures during electromagnetic launch [10]. This equation was solved with the help of the finite difference method (although no convergence criterion was available) for a copper fibre armature with a rail-armature interface length of 10 mm, launched with a 20 mm square-bore accelerator. The current profile, which mimics a capacitor bank discharge, shows a linear decrease to 70% of its initial value I(t = 0) in 3 ms and the armature velocity increases linearly from 0 to 3 km/s in this time interval. Hughes and Young used contour C'_1, given in Figure 5.1, to calculate the muzzle voltage for this launch. The rise of the temperature in the armature, caused by Joule heating, and induction contributions to V_m were not considered. Figure 5.2 shows the muzzle voltage as obtained by Hughes and Young. The resistivity of the armature material was taken equal to $5 \cdot 10^8$ Ωm. The muzzle voltage was found to

be proportional to the initial current. In these calculations we took $I(t = 0) = 494$ kA.

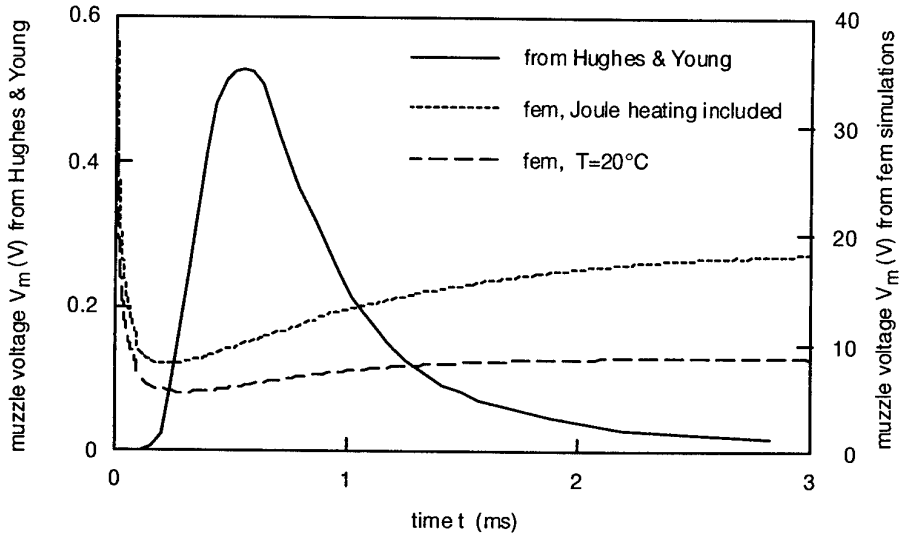

Figure 5.2: Muzzle voltage versus time, calculated by Hughes and Young [10] and with our method, which is incorporated in the finite-element computer code ET-code(denoted by 'fem').

In the 2-D representation of the rail accelerator and armature, the electric field **E** and the magnetic induction **B** are found by solving a diffusion-type equation for the magnetic field. Although the magnetic field at the front edge of the armature is set equal to zero in order to solve the governing equation for the magnetic induction, the current density, which equals the curl of the magnetic field, can have a finite value in the armature near the leading edge in this representation. However, comparison with the results of 3-D computations shows that the current densities at the front edge of the armature, obtained with the two-dimensional diffusion equation, are probably too small [11]. Therefore, V_m is calculated with our method for the electromagnetic launch circumstances studied by Hughes and Young by evaluating the integral (see eq. 5.2) along path C'_2. The local rise of the resistivity in the armature due to Joule heating is taken into account in this simulation.
Figure 5.2 shows that there are no similarities between the muzzle voltage calculated by Hughes and Young and with our method: both the profile and the magnitude are very different. Apart from the high values near $t = 0$ (which are due to the 'step function'-like behaviour of the current at $t = 0$), the muzzle voltage resulting from our method resembles measurements of V_m in launch experiments where capacitor banks are used.
In earlier studies, it has been concluded that the rise of the resistivity due to Joule heating has a large influence on the current distribution in the armature [1], [2], [4], [5]. Figure 5.2 also shows that a similar conclusion holds for the muzzle voltage.

5.3 Comparison with results of armature test bed experiments and electromagnetic launches

In order to validate the developed method, the muzzle voltage calculated with the computer code is compared with results of measurements during an armature test bed experiment and an electromagnetic launch experiment, both performed with a multi-fibre solid brush armature. The geometry of this copper armature is depicted in Figure 5.1.

Recently a device for testing armatures, rail accelerators and rail accelerator diagnostics under static conditions, the so-called armature test bed, has been developed at the TNO-PML Pulse Physics Laboratory. A comprehensive description of this device can be found in [12]. Essentially, it is a short rail accelerator with a square bore of 20 mm in which the armature under study is held fixed.

During armature test bed experiment A_300195_2, the muzzle voltage was measured with a 12-bit waveform recorder at a sampling rate of 1 MHz and a range of ± 24 V. The current pulse, provided by a capacitor bank, the measured muzzle voltage and the muzzle voltage calculated with our method are shown in Figure 5.3. The resemblance of the behaviour of $V_{m,exp}$ and $V_{m,sim}$ is clear, although the sharp bend in the measured muzzle voltage at t = 1.2 ms is absent in $V_{m,sim}$.

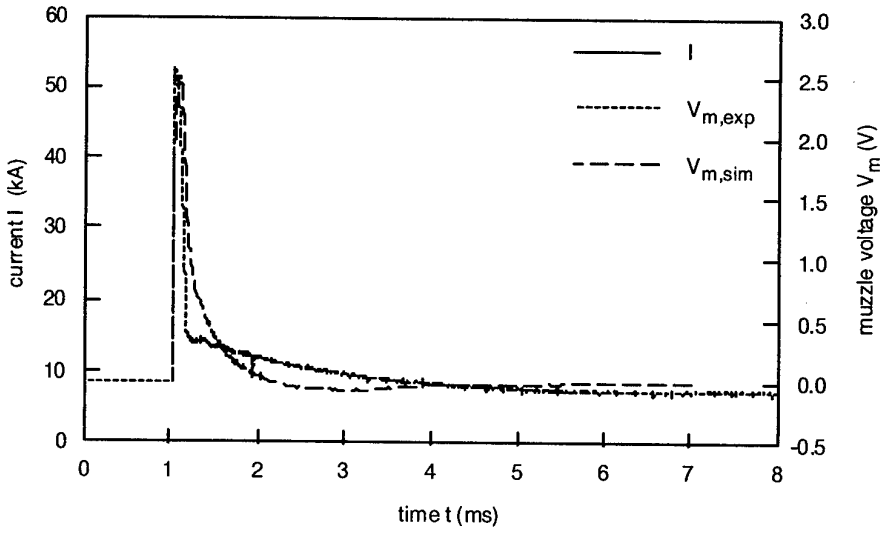

Figure 5.3: The measured current pulse I, the measured muzzle voltage $V_{m,exp}$ and the muzzle voltage $V_{m,sim}$ calculated with our method for armature test bed experiment A_300195_2.

The current pulse and the armature velocity of experiment E_110593 performed at the Pulse Physics Laboratory with the copper fibre armature in a 2.37 m rail accelerator with a 20 mm square bore, are shown in Figure 5.4. In the 250 ms preceding the actual current pulse, the current through the armature increases linearly from zero to 27.8 kA. The armature velocity is measured with B-dot probes and with a velocity interferometer.

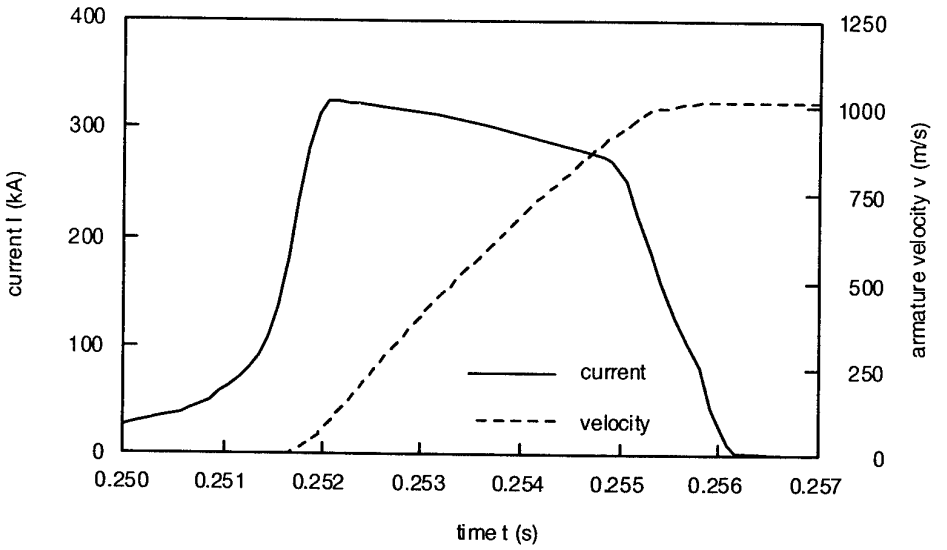

Figure 5.4: The measured current pulse and armature velocity of experiment E_110593.

Figure 5.5 shows the experimentally determined muzzle voltage $V_{m,exp}$ and the muzzle voltage calculated with the 2-D finite element computer code $V_{m,sim}$. At t = 254.7 ms, the muzzle voltage rises to a value of approximately 130 V. The generally accepted opinion is that this sudden rise of V_m is caused by a transition of the solid armature to a hybrid one, i.e. an armature which is partly solid and partly fluid (melted metal), vapour or plasma. In the model on which the computer code is based, the resistivity of the mesh elements increases quickly when the temperature in these elements reaches the melting temperature of the material considered. The spike on $V_{m,sim}$ at t = 253.5 ms is due to this sudden increase of the resistivity of the elements at the armature trailing edge. Since no model for the transition is included in the computer code used here, the sudden rise of V_m observed in the experiment at the transition time is absent in the simulated muzzle voltage.

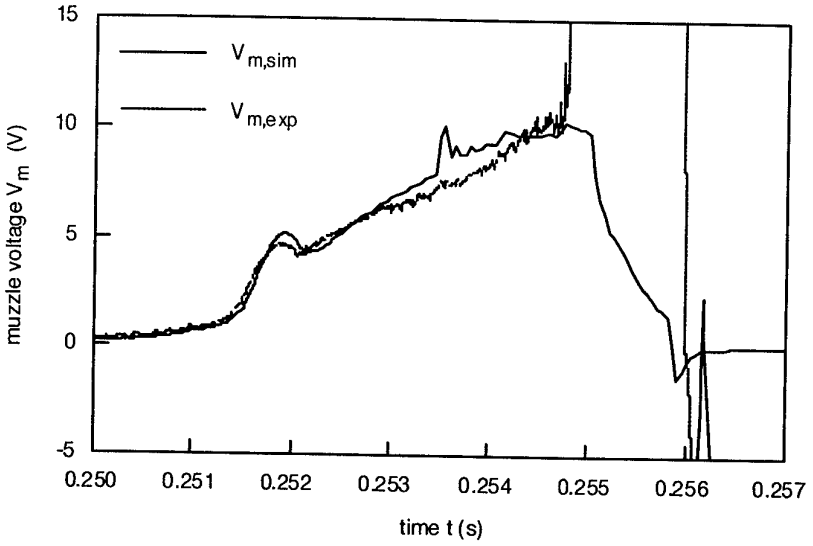

Figure 5.5: Experimentally determined muzzle voltage $V_{m,exp}$ and simulated muzzle voltage $V_{m,sim}$ for launch experiment E_110593.

The contributions to $V_{m,sim}$ are shown in Figure 5.6. The IR-drop along the trailing edge of the armature is denoted by v1. The contributions due to the IR-drop over the rail-armature interfaces, i.e. the voltage differences between the front edge and the trailing edge of the armature, are denoted by v2. The induction contributions from the region at the muzzle side of the armature, v3, and from the armature region, v4, are only significant when the current through the armature changes quickly.

The velocity of the armature influences the current density distribution during the launch cycle to a large extent. This effect is known as the velocity skin effect. To show the influence of this effect on V_m, the muzzle voltage is determined in a simulation of a motionless armature (see Figure 5.7). The same fibre armature and current profile are used as in the preceding simulation. It is clear from Figures 5.6, 5.7 and 5.8 that the velocity skin effect has a large influence on the value of the IR-drop at the trailing edge of the armature measured along the fibre direction, i.e. contribution v1.

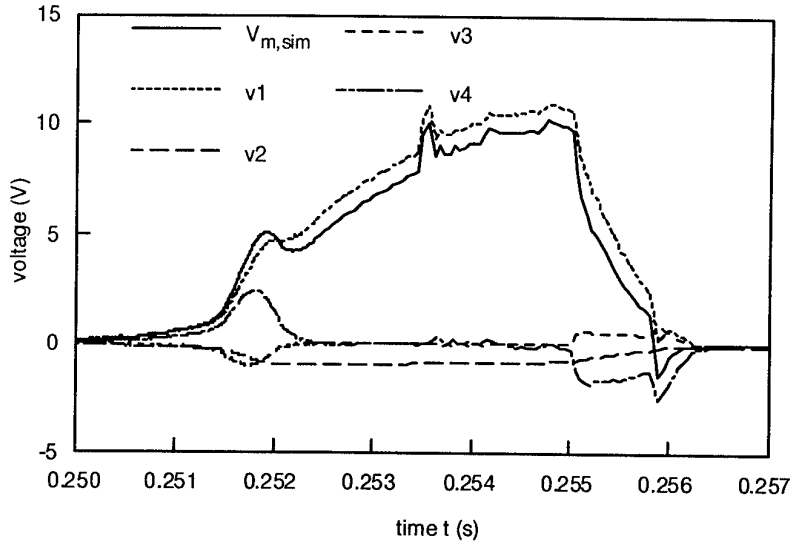

Figure 5.6: Contributions v1, v2, v3 and v4 to $V_{m,sim}$ for experiment E_110593.

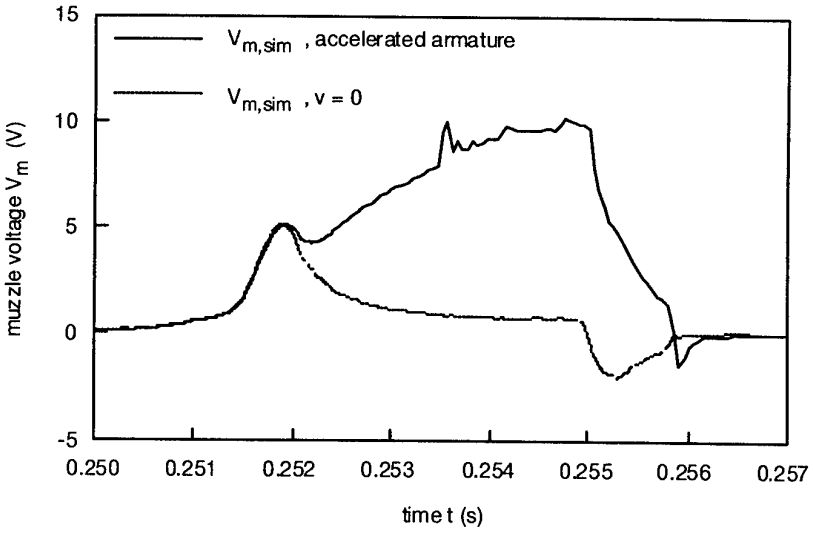

Figure 5.7: Comparison of the muzzle voltages for experiment E_110593 with an accelerated armature and with a motionless armature.

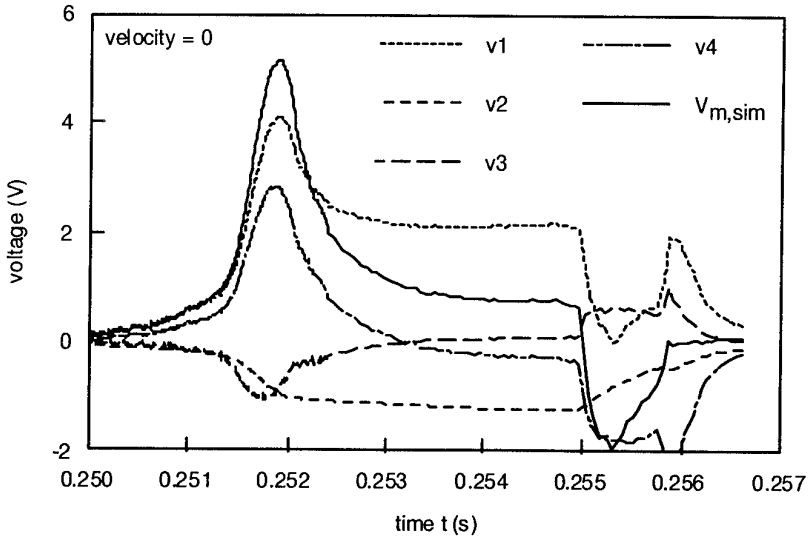

Figure 5.8: Contributions v1, v2, v3 and v4 to $V_{m,sim}$ for experiment E_110593 with a motionless armature.

5.4 A simple model for transitioning fibre armatures

In the multi-fibre solid brush armature launch experiment E_110593, described in the previous section, the rapid rise of the measured muzzle voltage at t = 0.2548 s, due to the armature transition, is clearly observed. The computer code has been extended with a simple model for the transition, based on the melt-wave concept proposed by P.B. Parks [13]: when the local temperature in the armature material becomes equal to the melting temperature of the material under consideration, the region with this temperature is removed from the armature. In the muzzle voltage calculation, a path C' is chosen which avoids this region at any point in time. Since the removal of armature material starts at the back of the armature, the path C' moves gradually from C'_2 to C'_1 (see Figure 5.1). Figure 5.9 shows the current distribution in the armature and the adjacent part of the rail at t = 0.254 s. The removed part of the armature is coloured black.

Figure 5.10 shows the muzzle voltage calculated in the simulations with and without the transition model, and the measured muzzle voltage of experiment E_110593. The seven 'spikes' on the muzzle voltage calculated with the transition model, V_{m,sim_tr}, are due to the melting and consequent removal of large parts of the armature and can be regarded as numerical artefacts.

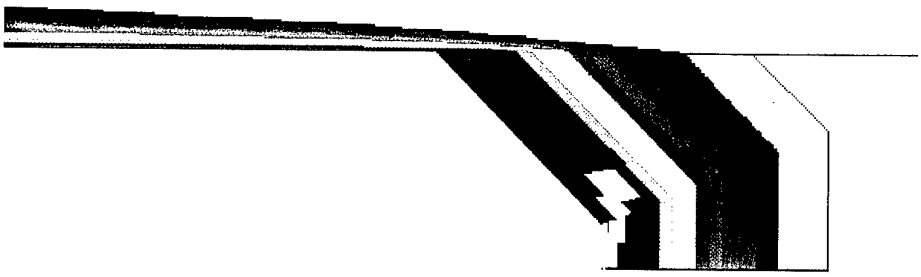

Figure 5.9: Current distribution in a part of the rail and the armature at t = 0.254 s (v = 695 m/s). The removed armature part at the rear is depicted in white.

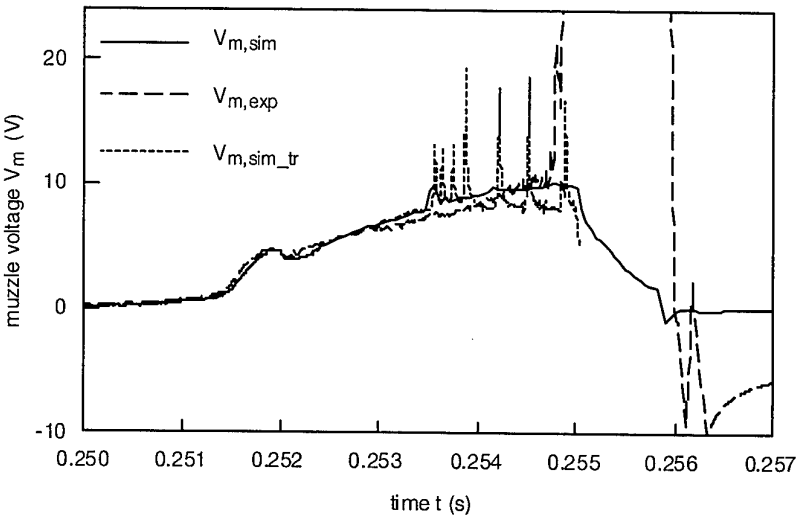

Figure 5.10: Muzzle voltage for experiment E_110593, calculated with and without the transition model (resp. V_{m,sim_tr} and $V_{m,sim}$), and the experimentally determined muzzle voltage $V_{m,exp}$.

At t = 0.255 s, when the current through the armature is decreasing rapidly, only half of the armature has melted according to the transition model. Since the successive appearance of the liquid, vapour and plasma phases during a transition is replaced by the removal of armature material in the model, one expects that the model will predict a transition in an earlier stage of the launch process than will occur in an actual experiment. However, no transition is predicted for launch experiment E_110593. The rapid rise of the muzzle voltage observed in launch experiment E_110593 cannot be explained as being the result of a transition of electrothermal origin.

6 A frictional heating model

In the simulations described in the previous chapters and in reports [1] and [2], the only heat source taken into account is the Joule heating. According to the results of these simulations, melting of the armature material starts not at the rail-armature interface, but in the bulk of the armature, because the fibre tips are cooled by the cold rail during the acceleration process. However, from the remnants of the fibre armatures which are recovered after electromagnetic lauch experiments it can be concluded that the fibre tips melt during launch (see for example [14]). A possible explanation is melting due to mechanical friction. In this chapter, the heating of the armature due to friction is considered, and the influence of frictional heating on the temperature distribution during electromagnetic launch processes is studied by means of computer simulations.
The electromagnetic acceleration of U-shaped copper multi-fibre solid brush armatures with a 20 mm square bore accelerator with copper rails is simulated. The armature geometry and the element mesh used in the simulations is given in Figure 6.1. The armature interface length is 15 mm and the width is 13 mm. The current and the velocity profile used in the simulations are given in Figure 6.2. The armatures start to move when the current is equal to 125 kA. In order to be able to compare the results of the simulations mutually, it is assumed that the friction influences only the temperature distribution and not the velocity.

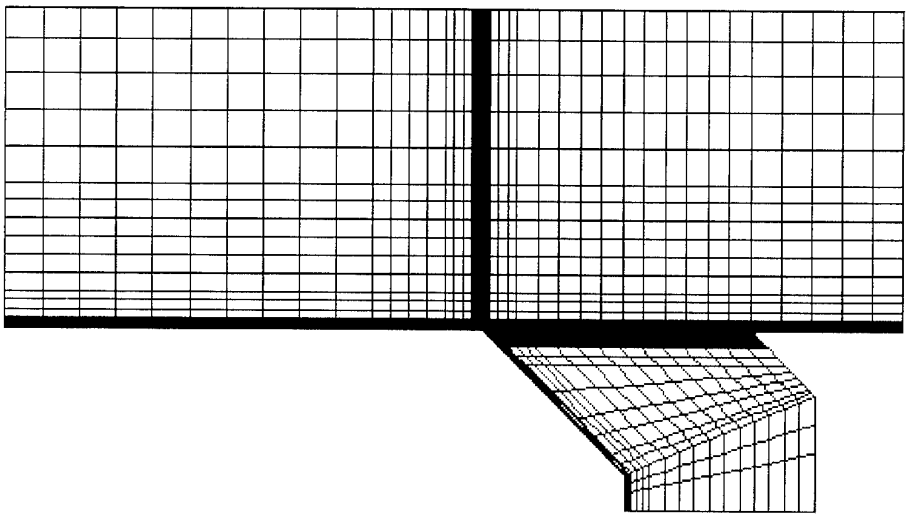

Figure 6.1: Armature geometry and element mesh.

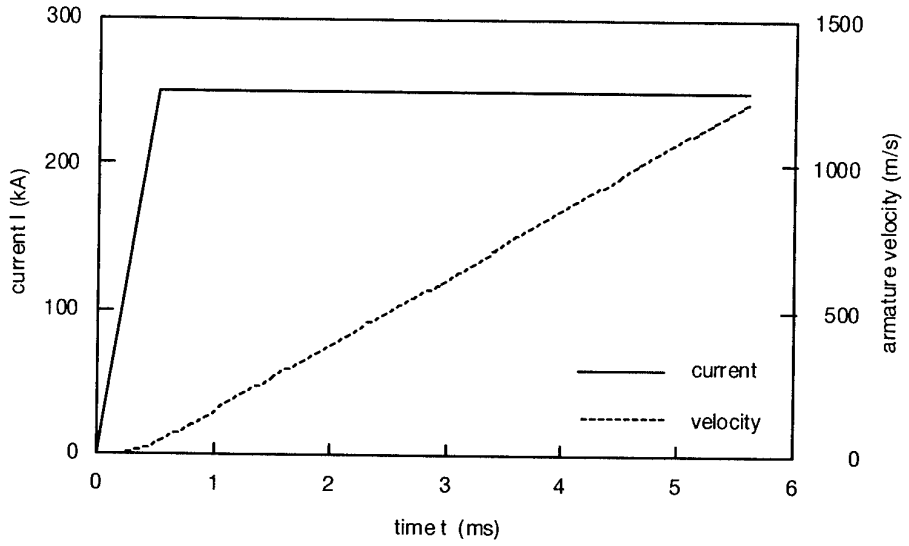

Figure 6.2: Current and velocity profile.

The heat flux **q** due to friction at the rail-armature interface is given by

$$q = C_f p^{(e)} v \; n \tag{6.1}$$

with

C_f = the coefficient of friction
$p^{(e)}$ = the pressure at the interface
v = the armature velocity
n = the normal vector at the interface

In the frictional heating model used in the simulations, the coefficient of friction is chosen equal to 0.2, and the pressure at the interface is taken proportional to the pressure on the interface of a finite element of the armature situated along the interface

$$p^{(e)} \propto \left(\int_{V^{(e)}} J \times B dV \right)_{\perp} \tag{6.2}$$

Here, **J** and **B** are the current density and the magnetic induction, respectively. The Lorentz force density is integrated over the finite element volume $V^{(e)}$. The total friction force F_f is assumed to be equal to 10% of the Lorentz force in the direction of the acceleration F_L

$$F_f = \int_{interface} p^{(e)} dO = 0.1 F_L \tag{6.3}$$

The chosen values for the coefficient of friction and the ratio of the friction force and the Lorentz force are realistic values for electromagnetic launch processes of copper fibre armatures with accelerators with copper rails [15].

Figure 6.3 shows the pressure profile along the rail-armature interface at four points in time during the acceleration calculated with this model. The resulting temperature distribution, denoted by 'h2', is given in Figure 6.4. In this figure the temperature distribution calculated in a simulation in which the Joule heating is neglected, identified by 'h4', is also shown. The heat sources in the simulations are summarized in Table 6.1.

Table 6.1: Heat sources in the simulations.

identification	heat source(s)
h0	Joule heating
h1	Joule heating, degradation of insulation
h2	friction and Joule heating
h4	friction
h5	friction with preload force and Joule heating
h6	friction with preload force

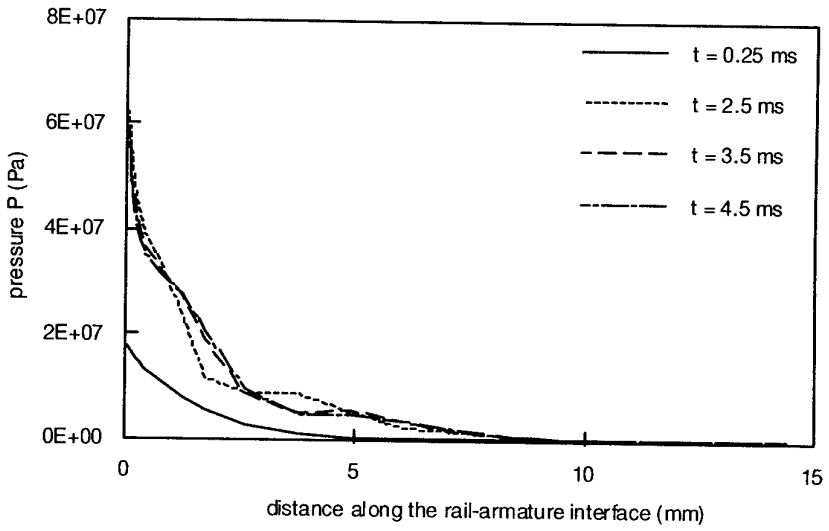

Figure 6.3: Pressure along the interface in simulation h2.

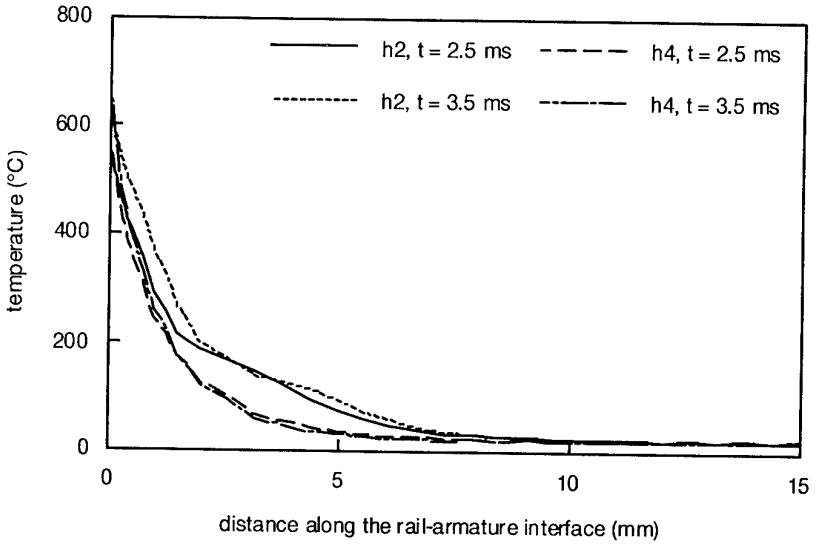

Figure 6.4: Temperature distribution along the interface from the simulation with frictional heating and Joule heating (h2) and the simulation in which only heating due to friction is included (h4). The coefficient of friction C_f is chosen equal to 0.2.

The temperature distributions in the simulations h2 and h4 can be compared with the temperature distributions in simulations of similar acceleration processes in which the coefficient of friction is equal to zero. For this purpose we consider two simulations, in which the only heat source is the Joule heating. In one of these simulations, h0, the electrical insulation of the fibres remains optimum and in the other simulation, h1, the gradual loss of the electrical insulation of the fibres between 150 °C and 250 °C due to melting of the insulation material is taken into account (see also [2], Chapter 4).

Figures 6.5 and 6.6 show the temperature profiles at t = 2.5 ms and t = 3.5 ms found in these four simulations along the fibres at 0.1 mm from the trailing side of the armature. The temperature distributions in the armature and the adjacent part of the rail at t = 3.5 ms are shown in Figures 6.7 - 6.10. The highest temperature is denoted by red and the lowest temperature of 20 °C (the starting temperature in the simulations) by blue.

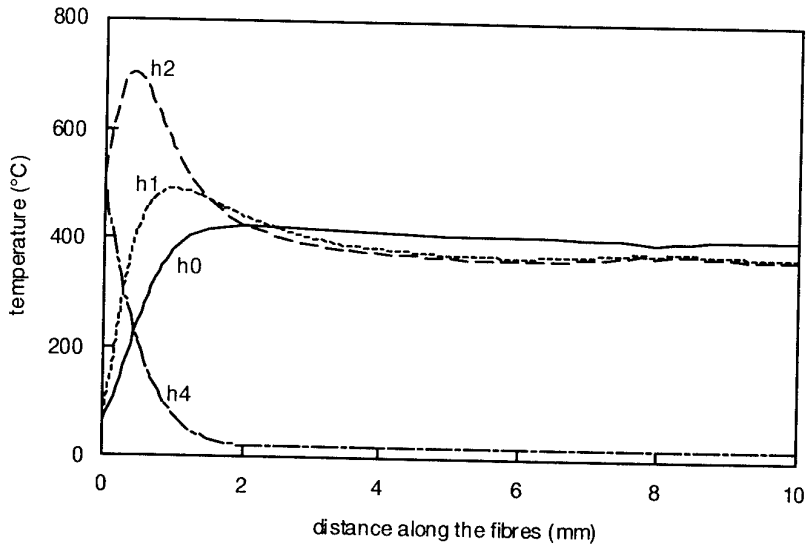

Figure 6.5: Temperature profiles along the fibres at 0.1 mm from the trailing side of the armature in the simulations h0, h1, h2 and h4 at t = 2.5 ms (v = 497 m/s).

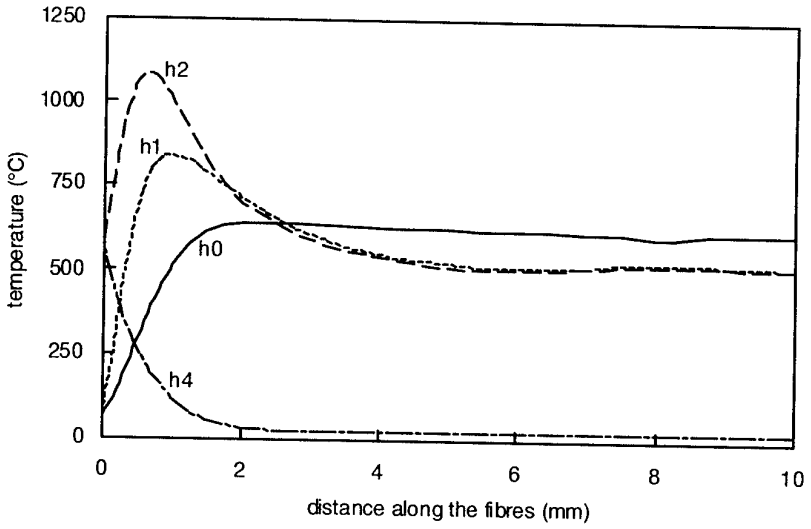

Figure 6.6: Temperature profiles along the fibres at 0.1 mm from the trailing side of the armature in the simulations h0, h1, h2 and h4 at t = 3.5 ms (v = 728 m/s).

Figure 6.7: Temperature distribution in the armature and the rail at t = 3.5 ms (v = 728 m/s) in the simulation with frictional heating and Joule heating (h2). The highest temperature, found at the red spot, is 1083 °C, the melting temperature of copper.

Figure 6.8: Temperature distribution in the armature and the rail at t = 3.5 ms in the simulation with only frictional heating (h4). The highest temperature is 657 °C.

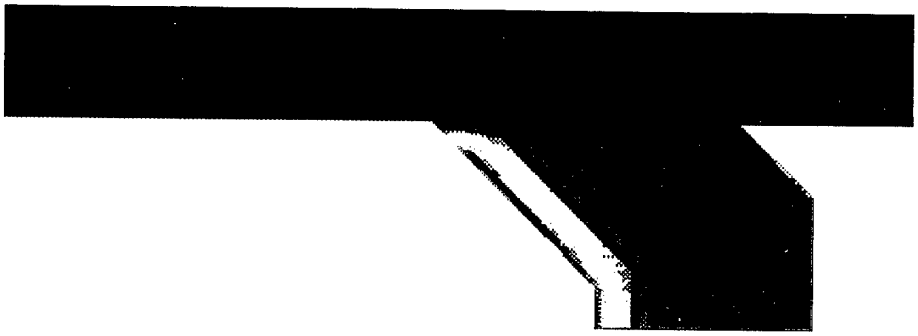

Figure 6.9: Temperature distribution in the armature and the rail at t = 3.5 ms in the simulation with only Joule heating (h0). The highest temperature is 643 °C.

Figure 6.10: Temperature distribution in the armature and the rail at t = 3.5 ms in the simulation with Joule heating and melting of the fibre insulation (h1). The highest temperature is 843 °C.

In order to study the influence of frictional heating due to the preload force, two simulations similar to the simulations described above are executed. In these simulations, a preload force of 635 N is assumed, which results in an extra pressure contribution p_{plf}. This pressure contribution, which is supposed to be independent from the position along the interface, is added to the position dependent pressure $p^{(e)}$ in the equation for the heat flux (6.1). This simulation, identified by h5, is equal to simulation h2, apart from the added pressure contribution p_{plf} (see also Table 6.1). In the simulation h6, only the frictional heating including the preload force contribution is taken into account.
The temperature profile at t = 3.5 ms along the fibres at 0.2 mm from the trailing side of the armature in the simulations h2, h4, h5 and h6 is shown in Figure 6.11. In the simulation h5, the melting temperature of copper (1083 °C) is reached. The temperature profile from this simulation in Figure 6.11 has a small plateau at a distance of 0.7 mm along the fibres due to the absorption of the heat of melting. Figure 6.12 shows the temperature profile along the interface.

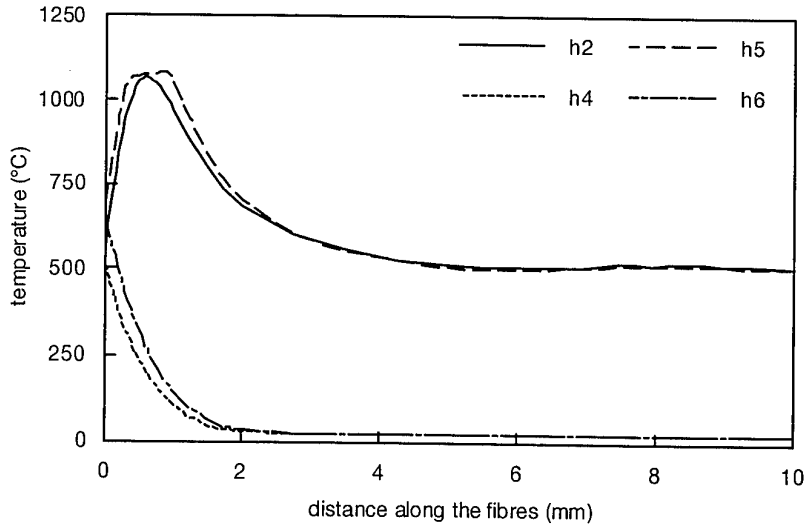

Figure 6.11: Temperature profile along the fibres at 0.2 mm from the trailing side of the armature in the simulations h2, h4, h5 and h6 at t = 3.5 ms.

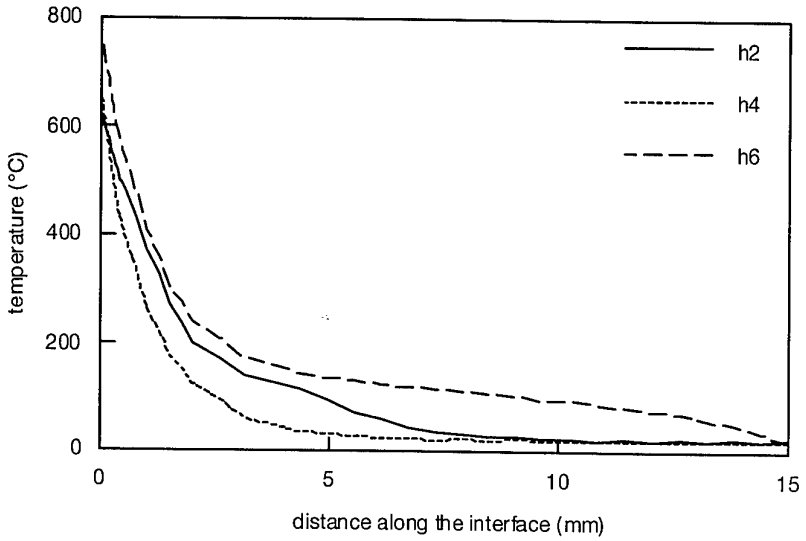

Figure 6.12: Temperature profile along the interface at t = 3.5 ms in the simulations h2, h4 and h6.

Figure 6.13: Temperature distribution in the armature and the rail at t = 3.5 ms in the simulation with Joule heating and frictional heating including the contribution due to the preload force (h5). The highest temperature is 1083 °C, i.e. the melting temperature of copper.

Figure 6.14: Temperature distribution in the armature and the rail at t = 3.5 ms in the simulation with frictional heating including the contribution due to the preload force (h6). The highest temperature is 774 °C.

Although it is very difficult to obtain experimental values for the parameters used in the frictional heating model, i.e. the coefficient of friction, the friction force and the preload force, we conclude from the results presented in this chapter that the melting of the fibre material of the armature at the rail-armature interface can be explained as being caused by the combination of Joule heating and frictional heating. By this mechanism, a melted layer at the interface can occur. This effect is even enhanced by the influence of the preload force on the frictional heating.

7 Conclusions

In this report, recent results of simulations of the electromagnetic acceleration process in a rail accelerator with the 2-dimensional electrothermal finite element computer code 'ET-code' are presented, and three extentions of the code, being the muzzle voltage calculation, the melt-wave model and the frictional heating model, are described. In order to obtain a uniform current distribution in the solid armature during launch, necessary for postponing the transition of such an armature to a hybrid one, three possible methods are investigated, i.e. the application of a resistive layer on the rails, the use of fibre armatures with fibre tips of a different material and the lengthening of the armature.

It has been found that the application of rails with a resistive layer in launches with monobloc armatures can increase the skin depth in the armature. However, the performance of a chosen rail layer-armature combination depends to a large extent on the material properties of the materials used. Because the influence of resistively layered rails on the current distribution in fibre armatures is not clear, more study on the combination of fibre armatures and resistively layered rails is necessary.

The launch performance of copper and molybdenum fibre armatures with fibre tips of aluminum, copper or molybdenum has been investigated. Although the current density in the tipped fibre armatures with a copper bulk is more homogeneous than in a copper fibre armature, melting and hence the transition of these armature starts at an earlier stage of the launch process. The current distribution in tipped fibre armatures with a bulk of molybdenum is determined by the properties of the bulk material. The use of an aluminum tipped fibre armature with a molybdenum bulk is probably interesting in order to obtain a fluid interface layer of melted aluminum during launch.

With the help of a new design for fibre armatures, the segmented fibre armature, the influence on the current distribution during launch of the armature lengthening has been investigated for U-shaped 45° copper and molybdenum armatures and launch parameters characteristic of the electromagnetic launch experiments at the Pulse Physics Laboratory. The optimal armature interface length of copper fibre armatures is between 7.425 mm and 14.85 mm for these launch parameters. Segmented copper fibre armatures with an interface length of 14.85 mm were investigated experimentally at the Pulse Physics Laboratory. For the molybdenum segmented fibre armatures, the optimal interface length is found to be longer than 37.125 mm.

A method to calculate the muzzle voltage during a simulated electromagnetic launch of multi-fibre solid brush armatures with the 2-D representation of a rail accelerator, is described in Chapter 5. It is pointed out that the contour of the integral of the electric field should be chosen along the trailing edge of the armature. An estimation of the induction contributions shows that these contributions are only significant when the breech current changes rapidly. Although 2-D simulations are used, the resulting muzzle voltages for armature test bed experiments and

launch experiments with solid fibre armatures bear much resemblance to the experimentally determined muzzle voltages. With a simple model for the transition of the armature, based on the melt-wave concept, it is concluded that the rapid rise of the muzzle voltage observed in launch experiment E_110593 cannot be explained as being a transition of electrothermal origin of a fibre armature.
From the simulation results with the frictional heating model, in which a position dependent pressure contribution along the rail-armature interface and the preload force are included, can be concluded that melting of the fibre tips at the interface due to friction is possible. This agrees with the conclusions drawn from visual inspection of armature remnants recovered after electromagnetic launch experiments. In the models for the transition of fibre armatures and for the electrothermal behaviour of hybrid armatures which will be developed in the continuation of the electromagnetic launch research, frictional heating must be included since it plays an important role in the heating and melting of the armature at the interfaces with the rails.

8 References

[1] Schoolderman, A.J.,
'Computer simulations of the electrothermal behaviour of armatures during electromagnetic launch. Part 1: Solid, one-component armatures',
TNO-report PML 1991-80, September 1991.

[2] Schoolderman, A.J.,
'Computer simulations of the electrothermal behaviour of armatures during electromagnetic launch. Part 2: Multi-fibre solid brush armatures',
TNO-report PML 1993-A77, December 1994.

[3] Long, G.C.,
'Fundamental limits to the velocity of solid armatures in railguns',
Ph.D. thesis, The University of Texas at Austin, August 1987.

[4] Schoolderman, A.J.,
'Two-dimensional electrothermal modelling of multi-fibre solid brush armatures',
paper no. p301 presented at the 4th European Symposium on Electromagnetic Launch Technology, May 2-6, 1993, Celle, Germany.

[5] Schoolderman, A.J.,
'Performance predictions for electromagnetic launching with multi-fibre solid brush armatures and resistively layered rail accelerators',
IEEE Trans. Magn. 31 (1995), 651-656.

[6] Weldon, W.F., Woodson, H.H. and Long, G.C.,
'Method and construction for control of current distribution in railgun armatures',
U.S. patent 4,953,441, September 4, 1990.

[7] James, T.E.,
'Performance criteria for EM rail launchers with solid or transition armatures and laminated rails',
IEEE Trans. Magn. 27 (1991) 482-487.

[8] Dreizin, Y.A.,
'Solid armature performance with resistive rails',
IEEE Trans. Magn. 29 (1993) 798-803.

[9] Long, G.C. and Weldon, W.F.,
'Limits to the velocity of solid armatures in railguns',
IEEE Trans. Magn. 25 (1989) 347-352.

[10] Hughes, W.F. and Young, F.J.,
'Diffusion skin effects in ultrahigh velocity laminated current collectors',
Wear 78 (1982), 171-187.

[11] Keefer, D., Taylor, J. and Crawford, R.,
'The electromagnetic force in railguns',
paper no. p1503 presented at the 4th European Symposium on Electromagnetic Launch Technology, May 2-6, 1993, Celle, Germany.

[12] Koops, M. and Karthaus, W.,
'Test bed for the evaluation of solid armature concepts',
presented at the 5th European Symposium on Electromagnetic Launch Technology, April 10-13, 1995, Toulouse, France.

[13] Parks, P.B.,
'Current melt-wave model for transitioning solid armature',
J. Appl. Phys. 67 (1990), 3511-3516.

[14] Karthaus, W., Zeeuw, W.A. de and Kolkert, W.J.,
'On the design and testing of solid armatures for rail accelerator applications',
IEEE Trans. Magn. 27 (1991) 308-313.

[15] Koops, M.,
'Study of the in-bore acceleration process in electromagnetic rail launchers using velocity interferometry',
paper presented at the 3th European Symposium on Electromagnetic Launch Technology, April 16-18, 1991, London, UK.

9 List of symbols

d	skin depth	(m)
l	armature length	(m)
n	normal vector	
$p^{(e)}$	pressure at the interface	(Pa)
p_{plf}	pressure due to the friction force	(Pa)
q	heat flux (vector)	(W/m^2)
r	packing fraction (for fibre armatures)	
t	time	(s)
v	velocity	(m/s)
$v1, v2, v3, v4$	contributions to the muzzle voltage	(V)
w	thickness (of a resistive layer on the rails)	(m)
C_f	coefficient of friction	
B	magnetic induction (vector)	(T)
E	electric field (vector)	(V/m)
F_f	friction force	(N)
F_L	Lorentz force	(N)
I	current	(A)
J	current density (vector)	(A/m^2)
O	surface	(m^2)
$V^{(e)}$	volume of a finite element	(m^3)
V_m	muzzle voltage	(V)
α	trailing edge angle (for U-shaped armatures)	(°)
ρ_{Cu}	resistivity of copper	(Ωm)
ρ_{rl}	resistivity of the resistive layer on the rails	(Ωm)

10 Authentication

W. Karthaus
Project leader

Dr. A.J. Schoolderman
Author

REPORT DOCUMENTATION PAGE
(MOD-NL)

1. DEFENCE REPORT NO. (MOD-NL)	2. RECIPIENT'S ACCESSION NO.	3. PERFORMING ORGANIZATION REPORT NO.
TD96-0406		PML 1996-A79
4. PROJECT/TASK/WORK UNIT NO.	**5. CONTRACT NO.**	**6. REPORT DATE**
233494015.003	A87KL046	November 1996
7. NUMBER OF PAGES	**8. NUMBER OF REFERENCES**	**9. TYPE OF REPORT AND DATES COVERED**
42 (excl. RDP & distribution list)	15	Final

10. TITLE AND SUBTITLE

Computer simulations of the electrothermal behaviour of armatures during electromagnetic launch
Part 3: Miscellaneous 2-D simulation results

11. AUTHOR(S)

Dr. A.J. Schoolderman

12. PERFORMING ORGANIZATION NAME(S) AND ADDRESS(ES)

TNO Prins Maurits Laboratory, Pulse Physics Laboratory, P.O. Box 45, 2280 AA Rijswijk, The Netherlands
Visiting address: Schoemakerstraat 97, 2628 VK Delft, The Netherlands

13. SPONSORING AGENCY NAME(S) AND ADDRESS(ES)

DMKL/WO, P.O. Box 90822, 2509 LV The Hague, The Netherlands

14. SUPPLEMENTARY NOTES

The classification designation Ongerubriceerd is equivalent to Unclassified.

15. ABSTRACT (MAXIMUM 200 WORDS (1044 BYTE))

Recent results of simulations of the electromagnetic acceleration process with the 2-dimensional electrothermal finite element computer code ET-code are presented and three extentions of the code, the muzzle voltage calculation, the melt-wave model and the frictional heating model, are described. In order to obtain a uniform current distribution in the solid armature during launch, necessary for postponing the transition of the armature to a hybrid one, three possible methods were investigated, i.e. the application of a resistive layer on the rails, the use of fibre armatures with tipped fibres and the lengthening of the armature.

16. DESCRIPTORS	IDENTIFIERS
Computerized simulation Armatures Accelerators Electromagnetic launching Finite elements methods Computer programs	

17a. SECURITY CLASSIFICATION (OF REPORT)	17b. SECURITY CLASSIFICATION (OF PAGE)	17c. SECURITY CLASSIFICATION (OF ABSTRACT)
Ongerubriceerd	Ongerubriceerd	Ongerubriceerd

18. DISTRIBUTION AVAILABILITY STATEMENT	17d. SECURITY CLASSIFICATION (OF TITLES)
Unlimited Distribution	Ongerubriceerd

Distributielijst*

1*/2*	DWOO
3	DWOO
4	HWO-KL
5*	HWO-KLu
6*	HWO-KM
7	PHWO-KM
8	DMKL/T&WO, LKol. ir. E.J.H. Elstak
9	BMDO, Dr. Leonard Caveny
10	Bureau TNO-DO
11/13	Bibliotheek KMA
14	Lid Adviescommissie Pulsfysica, Prof. ir. J.A. Schot
15	Lid Adviescommissie Pulsfysica, Prof. dr. W.R. Rutgers
16*	Lid Instituuts Advies Raad PML, Prof. B. Scarlett, M.Sc.
17*	Lid Instituuts Advies Raad PML, BGen. Prof. J.M.J. Bosch
18*	Lid Instituuts Advies Raad PML, Prof. ir. K.F. Wakker
19	TNO-PML, Directeur; daarna reserve
20	TNO-PML, Directeur Programma; daarna reserve
21	TNO-PML, Hoofd Divisie Wapens en Wapenplatformen, Dr. R.R. IJsselstein
22	TNO-PML, Documentatie
23	TNO-PML, Archief
24	TNO PML-Pulsfysica, Hoofd, Dr. W.J. Kolkert
25	TNO PML-Pulsfysica, Archief
26	TNO PML-Pulsfysica, Documentatie
27	TNO PML-Pulsfysica, EML
28	TNO PML-Pulsfysica, PPR
29/30	Reserve

---

* De met een asterisk (*) gemerkte instanties/personen ontvangen uitsluitend de titelpagina, het management-uittreksel, de documentatiepagina en de distributielijst van het rapport.